Sains Malaysiana 51(12)(2022): 3949-3966
http://doi.org/10.17576/jsm-2022-5112-07

A Quinoline-Based Fluorescent Labelling for Zinc Detection and DFT Calculations

(Pelabelan Pendarfluor Berasaskan Kuinolina untuk Pengesanan Zink dan Pengiraan DFT)

Nur Syamimi Mohamad[1], Ling Ling Tan[1], Goh Choo Ta[1], Lee Yook Heng[2], Nadhratun Naiim Mobarak[2], Azwan Mat Lazim[2], Suhaila Sapari[3], Fazira Ilyana Abdul Razak[3] & Nurul Izzaty Hassan[2,*]

[1]*Southeast Asia Disaster Prevention Research Initiative (SEADPRI-UKM), Institute for Environment and Development (LESTARI), Universiti Kebangsaan Malaysia, 43600 UKM Bangi, Selangor Darul Ehsan, Malaysia*
[2]*Department of Chemical Sciences, Faculty of Science & Technology, Universiti Kebangsaan Malaysia, 43600 UKM Bangi, Selangor Darul Ehsan, Malaysia*
[3]*Department of Chemistry, Faculty of Science, Universiti Teknologi Malaysia, 81300 Skudai, Johor Bahru, Johor Darul Takzim, Malaysia*

Received: 8 June 2022/Accepted: 1 September 2022

ABSTRACT

8-carboxamidoquinoline derivatives were gradually investigated as zinc's label in resolving weak water solubility, poor membrane permeability, and difficulty measuring free Zn^{2+} ion in cells quantitatively. The potential of 2-oxo-2-(quinolin-8-ylamino)acid (OQAA) as zinc's label was prepared and characterized spectroscopically. Theoretical and experimental data of OQAA were compared and discussed. The optimized molecular structure, molecular orbital of HOMO-LUMO, energy band gaps, and molecular electrostatic potential (MEP) of OQAA were carried out using the DFT method with Becke-3-Parameter-Lee-Yang-Parr (B3LYP) and 6-31G(d,p) basis set. The intermolecular interaction energy of OQAA-Zn is calculated by using the hybrid method of GEN with a basis set of LANL2DZ for Zn^{2+} ion and DFT/6-31G(d,p) for OQAA ligand. OQAA exhibited remarkable and excellent fluorescence enhancement selective and qualitatively only for Zn^{2+} than other metal cations tested (Fe^{2+}, Cu^{2+}, Co^{2+}, Ni^{2+}, Hg^{2+}, Cd^{2+}) under a long wavelength. Job's plot and ^{1}H NMR titrations indicate OQAA-Zn^{2+} has a binding ratio at 1:1 stoichiometry (M_1L_1). Substantial shifting of amide N-H proton to higher chemical shift and intensity of the proton peak of N-H amide decrease abruptly implies that Zn^{2+} is binding to an amide. These changes confirmed interactions among the ligand OQAA and metal Zn^{2+} ion. As a result of the benefits discussed, OQAA could effectively and selectively optimize and fabricate for Zn^{2+} sensors.

Keywords: Density functional theory; fluorescent sensor; metal cation; zinc label; 8-carboxamidoquinoline

ABSTRAK

Bahan terbitan 8-karboksamidokuinolina semakin mendapat perhatian sebagai label zink dalam menyelesaikan masalah keterlarutan air yang lemah, kebolehtelapan membran yang lemah, dan kesukaran mengukur ion Zn^{2+} bebas dalam sel secara kuantitatif. Sebatian asid 2-okso-2-(kuinolina-8-ylamino) (OQAA) yang berpotensi sebagai label zink telah disintesiskan dan dicirikan secara spektroskopi. Data teori dan uji kaji OQAA dibandingkan dan dibincangkan. Struktur molekul yang dioptimumkan, orbital molekul HOMO-LUMO, jurang jalur tenaga dan potensi elektrostatik molekul (MEP) OQAA telah dijalankan menggunakan kaedah DFT dengan Becke-3-Parameter-Lee-Yang-Parr (B3LYP) dan set asas 6-31G(d,p). Seterusnya, tenaga interaksi antara molekul OQAA-Zn dihitung menggunakan kaedah hibrid GEN dengan set asas LANL2DZ untuk ion Zn^{2+} dan DFT/6-31G(d,p) untuk ligan OQAA. OQAA menunjukkan peningkatan pendarfluor yang luar biasa dan cemerlang secara selektif dan kualitatif hanya untuk Zn^{2+} berbanding kation logam lain yang diuji (Fe^{2+}, Cu^{2+}, Co^{2+}, Ni^{2+}, Hg^{2+}, Cd^{2+}) di bawah lampu UV gelombang panjang. Plot Job dan titrasi ^{1}H NMR menunjukkan OQAA-Zn^{2+} mempunyai nisbah pengikatan pada stoikiometri 1:1 (M_1L_1). Peralihan besar amida N-H proton kepada anjakan kimia yang lebih tinggi dan keamatan puncak proton amida N-H menurun secara mendadak memberi gambaran bahawa Zn^{2+} terikat pada amida. Perubahan ini mengesahkan terdapat interaksi antara ligan OQAA dan ion logam Zn^{2+}. Kesimpulannya, hasil kajian yang dibincangkan ini membuktikan sebatian OQAA ini boleh dilanjutkan dengan pengoptimuman dan fabrikasi sensor Zn^{2+} yang berkesan dan selektif.

Kata kunci: Kation logam; label zink; sensor pendarfluor; 8-karboksamidokuinolina; teori kefungsian ketumpatan

Introduction

Zn is the second most abundant transition metal in the human body and is well known for its various biological processes such as enzymatic reactions, gene expression, protein, DNA synthesis, growth and development, immune function, and wound healing (Basabe-Desmonts, Müller & Crego-Calama 2007; Shyamal et al. 2016). Therefore, chemical sensors and biosensors have recently received much attention (Al-Khalqi et al. 2021). Due to its $3d^{10}$ electronic structure, the fluorescence method has been preferred over other techniques for detecting zinc(II) ions due to its operational simplicity (Chen, Han & Liu 2007; Ponnuvel & Padmini 2016). A fluorophore probe will emit specific fluorescence upon the binding with Zn^{2+} ions. This probe will act as a transducer, known as a sensing matrix, that aids in enhancing signal transduction (Siti Shafura et al. 2019). Therefore, the design of this fluorophore probe is vital in developing a more selective and sensitive method for recognizing Zn^{2+} ions. Among various standard probes that have been studied are derivatives of coumarin (Shamsipur et al. 2001), zinpyr (Urano et al. 2005), aminoquinoline (Gupta, Jain & Maheshwari 2006), zinquin (Tharmaraj & Pitchumani 2013), and Zinbo-5 (You et al. 2012).

Photoinduced electron transfer (PET), intermolecular charge transfer (ICT), and fluorescence resonance energy transfer (FRET) are among the plausible mechanism related to the strong binding of aminoquinoline to Zn^{2+} ion (Shi, Zhou & Zheng 2014). Amongst the aminoquinoline's probes, 6-methoxy-(8-p-toluenesulfonam-ido)quinoline (TSQ) derivative is the most efficient probe that has been used in the biological application (Bozym, Thompson & Fierke 2006). This TSQ forming metal complex($(TSQ)_2Zn$) at ratio 2:1. However, these derivatives displayed weak water solubility, poor membrane permeability, and difficulty quantitatively measuring free Zn^{2+} ions in cells (Dong et al. 2017).

Several attempts were made to address TSQ's low water solubility, including switching 8-aminoquinoline-based derivatives into 8-carboxamidoquinolines-based derivatives as zinc's fluorophore (Dong et al. 2014; Fu et al. 2019; Li et al. 2018; Park et al. 2015; Song & Zhang 2019; Yue et al. 2015; Zhang et al. 2008). However, based on our prior review of these derivatives, specific interferences made it challenging to distinguish between zinc ions and other competing cation metals, including Cd^{2+}, Cu^{2+}, Co^{2+}, Ni^{2+}, and Hg^{2+} to $3d^{10}$ electronic configurations (Mohamad et al. 2021). Other than that, to the best of our knowledge, no studies successfully reported qualitative detection of Zn^{2+} and other competitive metals using 8-carboxamidoquinolines-based labels.

To enhance the hydrophilicity of zinc fluorescent probes, Ma et al. (2011) disclosed a ratiometric fluorescent probe for zinc ions based on 8-carboxamidoquinoline with a carboxylic acid group that shows an intense fluorescence response upon the addition of Zn^{2+} in buffer water/ethanol (pH 7.24). The effectiveness of adopting probe 1 to determine Zn^{2+} in tap and river water samples has been proven. Furthermore, oxamide was thought to have excellent coordination aspects (symmetric and asymmetric, cis and trans) in forming metal complexes due to its exceptional coordination efficiency and structure diversification (Tian et al. 2016). Accordingly, other than N-atom and O-atom of amide coordinates favorably to Zn^{2+}, N-atom of quinoline and quinoline ring itself also showed strong complexation 8-Amidoquinoline Zn^{2+} binding by π-π intermolecular stacking ability (Czaplinska, Spaczynska & Musiol 2018).

Therefore, we are concerned with exploring an 8-carboxamidoquinolines-based label that combines 8-carboxamidoquinoline and carboxylic acid using oxamide's bridging like 2-oxo-2-(quinolin-8-ylamino) acid (OQAA) as fluorescent labeling for zinc detection. This derivative was previously reported as a component of aminoacridine oxamates salts (9-aminoacridine·3-quinolyl-NHCOCOOH) for antimicrobial activities (Petyunin & Sysun 1974). Thus, this study will explore another role of OQAA as a potentially fluorescent labeling sensor for zinc detection.

The theoretical calculations of OQAA interaction with zinc were calculated by the density functional theory (DFT) method using the B3LYP function with the 6-31G (d,p). The molecular electrostatic potential map illustrates the charge distributions of the molecule three-dimensionally. At the same time, the HOMO and LUMO energy gap could explain the eventual charge transfer interactions during the complexation (Khairul et al. 2016). As for examination of the interaction utilizing the BSSE approach has been recognized to suffer from a systematic and unphysical overestimation (Galano & Alvarez-Idaboy 2006; Jensen 2010). Therefore, one of the most well-known corrective methods limiting the inaccuracy when analyzing an intermolecular reaction with an incomplete basis set was the counterpoise (CP) parameter/keyword applied in calculating the hybrid GEN method (Lopes et al. 2010). As a whole of these studies,

this simple probe of OQAA could be used further to fabricate a fluorescent sensor of Zn^{2+} effectively.

Herein, we reported the design, spectral characteristic, binding, and computational studies of OQAA. Only two steps are required to synthesize this, which do not involve any catalyst or hazardous chemical like chloroacetyl chloride. Two simple steps were direct aminolysis and proceeded with a simple process of hydrolysis of the ester. Therefore, as part of our ongoing research, an investigation of OQAA was found to detect Zn^{2+} ions selectively and qualitatively under a long UV lamp (different colour changes of OQAA solution upon binding with Zn^{2+} and other metals). Aside from that, this label may prevent leakage during biological sensing as it has both hydrophobic and hydrophilic parts.

Materials and Methods

Materials and Instrumentations

The required chemicals (8-aminoquinoline, diethyl oxalate, potassium hydroxide, and hydrochloric acid) and analytical grade solvents (chloroform, dichloromethane, methanol, ethanol, tetrahydrofuran, and ethyl acetate) that have been used in synthesizing and experimenting with binding studies of 8-amidoquinoline's derivatives were attained from Aldrich, Merck, Fluka, and R&M without further purification. All the synthesized compounds were characterized by using spectroscopic techniques like Fourier Transform-Infrared (FTIR) spectroscopy, UV-Visible (UV-Vis) spectroscopy, and Nuclear Magnetic Resonance (NMR) spectroscopy, and Electrospray Ionization Mass Spectrometer (ESI-MS). FTIR spectra with an Agilent Cary 630 ATR-FTIR analyzer in the 4000–650 cm^{-1}. For NMR data, the spectra of ^{1}H-NMR (400 MHz) and ^{13}C-NMR (100.6 MHz) were collected by FT-NMR 400 MHz Advance 400 III HD Bruker. Internal standard tetramethylsilane (TMS, $Si(CH_3)_4$) was used as a reference, while deuterated chloroform ($CDCl_3$) and dimethyl sulfoxide ($(CD_3)_2SO$) were used as NMR's solvent. All NMR data were analyzed with ACD labs software. UV-Vis spectra were taken from the Shimadzu UV-1800 spectrophotometer using a quartz cell with a path length of 3 cm in DMSO. Next, ESI-MS were recorded in positive ion mode with Bruker micrOTOF-Q (Bruker Daltonics) spectrometer. The binding study of 8-Amidoquinoline towards Zn^{2+} ions was conducted by ^{1}H-NMR titration and fluorescence titration (Hitachi F-7000 spectrophotometer).

Synthesis of Ethyl 2-oxo-2-(quinolin-8-ylamino) Acetate EOQA (1)

A mixture of 8-aminoquinoline (1.0 g, 6.97 mmol) and diethyl oxalate (5 mL, 38.02 mmol) were added together at a ratio of 1:5. The mixture was swirled and refluxed for 90 min. Then, the resulting crude mixture was continued with further purification via column chromatography by using dichloromethane (DCM) as eluent. After removing DCM under reduced pressure, the EOQA compound was obtained as brown solid in 80% yield (1.36 g). M.p: 76.9-78.1°C. ^{1}H NMR (400 MHz, $CDCl_3$) δ (ppm): 11.32 (1H, s, N-H), 8.83-8.81 (1H, dd, J = 1.6, 6.8 Hz, HAr), 8.74-8.72 (1H, dd, J = 1.6, 4.0 Hz, HAr), 8.13-8.10 (1H, dd, J = 4.0, 8.4 Hz, HAr), 7.56-7.48 (2H, m, HAr), 7.44-7.41 (1H, dd, J = 1.6, 8.4 Hz, HAr), 4.45-4.39 (2H, q, J = 6.8 Hz, CH2), 1.43-1.39 (3H, t, J = 7.2 Hz, CH3). ^{13}C NMR (100.6 MHz, $CDCl_3$) δ (ppm): 160.7 (CO=O), 154.3 (CNH=O), 148.9 (CH aromatics-N), 138.7 (C aromatics-N), 136.3 (CH aromatics), 133.0 (C aromatics-NH), 127.9 (C aromatics), 127.2 (CH aromatics), 123.3 (CH aromatics), 121.9 (CH aromatics), 117.4 (CH aromatics), 63.6 (CH_2) and 14.1(CH_3). UV-Vis (nm): 244 and 324. FTIR-ATR $\bar{\upsilon}$ (cm^{-1}): 3306.1 (Secondary N-H amide), 1699.7 (C=O), 1528.2 (C=C aromatics), 1282.2 (CO-O) and 1162.9 (CO-O). ESI-MS: m/z calculated for $[C_{13}H_{12}N_2O_4 + Na]^+$: 267.0745, found 267.0749.

Synthesis of 2-oxo-2-(quinolin-8-ylamino)acetic Acid OQAA (2)

Different set of solvents such as methanol (MeOH), ethanol (EtOH), and a mixture of two solvent tetrahydrofurans (THF): MeOH at a ratio of 1:1 was prepared in 10 mL to attain better yield. EOQA (122.12 mg, 0.5 mmol) was stirred with the chosen solvent and proceeded to be stirred overnight or refluxed at 70 °C for a stipulated time (according to the thin-layer chromatography (TLC) result). 3 mL of 1 N potassium hydroxide (KOH) was added dropwise into the solution during the reflux. After cooling, the solution was acidified to pH 2 with the addition of 3 N HCl at 0 °C before being further extracted with liquid-liquid extraction (ethyl acetate). Subsequently, the combined organic layer will be dried over anhydrous sodium sulfate and evaporated to afford the final product of OQAA (Yield: 94.2 mg, 87%). M.p: 203.5-204.7 °C. ^{1}H NMR (400 MHz, $CDCl_3$) δ (ppm): 11.10 (1H, s, N-H), 8.85-8.45 (1H, dd, J = 1.6, 4.0 Hz, HAr), 8.99-8.97 (1H, dd, J = 1.6, 8.0 Hz, HAr), 8.68-8.65 (1H, dd, J = 1.2, 7.6 Hz, HAr), 7.79-7.74 (1H, dd, J = 1.2, 8.0 Hz, HAr), 7.71-7.64 (2H, m, HAr), OH is absent. ^{13}C NMR (100.6 MHz,

$CDCl_3$) δ (ppm): 162.1(COOH), 155.9 (CNH=O), 149.9 (CH aromatics-N), 138.3 (C aromatics-N), 137.3 (CH aromatics), 133.2 (C aromatics-NH), 128.3 (C aromatics), 127.5 (CH aromatics), 123.7 (CH aromatics), 123.1 (CH aromatics), and 116.5 (CH aromatics). FTIR-ATR $\bar{\upsilon}$ (cm^{-1}): 3448.8 (Secondary N-H amide), 3242.7 (O-H broad), 1688.5 (C=O), and 1498.4(C=C aromatics). UV-Vis (nm): 267 and 320. ESI-MS: m/z calculated for $[C_{11}H_8N_2O_3 + H]^+$: 216.0535, found 217.0600.

PRELIMINARY SCREENING OF OQAA WITH METAL SALTS

Diluted OQAA conducted preliminary screenings in DMSO/H_2O mixtures at 1 mM. All-metal tested $Cd(NO_3)_2 \cdot 4H_2O$, $Co(NO_3)_2 \cdot 6H_2O$, $CuSO_4 \cdot 5H_2O$, $NiCl_2 \cdot 6H_2O$, $FeSO_4 \cdot 7H_2O$, $HgCl_2$, and $(Zn(SO_4) \cdot 7H_2O)$ were prepared. Subsequently, OQAA: metal was mixed at a ratio of 1:1. The fluorescence changes under the long wavelength of the UV lamp (365 nm) were recorded before and after the mixing.

SAMPLE PREPARATION FOR BINDING STUDY WITH ZN(II) ION

Fluorescence titrations were conducted using OQAA diluted in DMSO/H_2O mixtures with water fractions of 50%. The concentration of OQAA was fixed to 3×10^{-4} M. Then, fluorescence titration proceeded to determine the stoichiometry of OQAA-Zn by using the equimolar stock of OQAA and $Zn(SO_4) \cdot 7H_2O$. All the fluorescence spectra were taken at room temperature. Job's plots were drawn by plotting fluorescence emission versus the molar fraction of OQAA-Zn. Next, complexometric titration between OQAA and $Zn(SO_4) \cdot 7H_2O$ were done by the same NMR instrument at ratio 1:0, 1:1, 1:2, 1:3, and 1:4. The changes in the chemical shift of each peak were observed for each proportion. As in fluorescence titration, this ^{1}H-NMR was conducted simultaneously at room temperature using the same instrument.

COMPUTATIONAL DETAILS

The targeted compounds were assessed at the density functional theory (DFT), Becke, 3-parameter, Lee-Yang-Parr (B3LYP) level with a basis set of 6-31G (d,p) employing the Gaussian 16 program package (Bukheet Hassan 2014; Salim et al. 2018) along with GaussView 6 as visualizer to examine the results graphically. The optimized molecular structure, molecular electrostatic potential (MEP), and complexation were computed in the gas phase. There were no symmetry limitations applied to the molecular geometry optimization. The calculated vibrational frequency values were scaled using a scale of 0.9613, and no imaginary frequencies were found. The UV-vis spectra of the optimized structure at the ground state were evaluated through the time-dependent functional theory (TD-DFT) based on the B3LYP functionals with the same basis set of 6-31G (d,p) level of theory in the gas phase. After optimizing the molecular geometry at the same level of theory, ^{1}H and ^{13}C NMR calculations were done using the gauge-invariant atomic orbital (GIAO) method in the gas phase at B3LYP/6–311+G(2d,p). Additionally, the DFT/B3LYP technique and a 6–31 G(d,p) basis set in the gas phase, optimization energy, HOMO-LUMO analysis, and molecular electrostatic potential (MEP) maps for OQAA were computed and visualized at the same level of theory. To obtain the energy interaction of the OQAA-Zn complexes, the structure was optimized using the GEN hybrid method with a keyword of counterpoise and basis set of LANL2DZ for metal Zn and DFT/6-31G(d,p) for the OQAA ligand. The basis set superposition error (BSSE) is evaluated, and the error is deducted from the uncorrected energy (DFT/B3LYP/GEN/LANL2DZ). The corrected interaction energy ($\Delta E_{corrected}$) is calculated by adding uncorrected energy ($\Delta E_{uncorrected}$) from optimization calculation to basis set superposition error (BSSE) energy (ΔE_{BSSE}) (Kadir, Abdul Razak & Haris 2020) (Equation 1).

$$\Delta E corrected, \text{kJ/mol} = \Delta E uncorrected + \Delta E BSSE \quad (1)$$

RESULTS AND DISCUSSION

Derivative of 8-amidoquinoline (OQAA) was synthesized by hydrolyzed EOQA with an acid-base reaction (Figure 1). The EOQA was prepared using the approach published by Tian et al. (2016). The chemical structure of the parent compound for both EOQA and OQAA were similar, with slight differences due to the ester group of EOQA being reduced to a carboxylic acid group to form OQAA.

CHARACTERIZATION OF 8-AMIDOQUINOLINE DERIVATIVES

A comparison of ^{1}H NMR between EOQA and OQAA in Figure 2(a) proves that the ester group (-OCH_2CH_3) peak of EOQA cannot be seen. Quartet (δ= 4.45-4.39) and triplet (δ= 1.43-1.39) splitting were missing in OQAA spectra. However, from ^{1}H NMR OQAA, the absence of one hydrogen peak is apparent because the hydrogen from labile protons like O-H, N-H, and S-H is sometimes

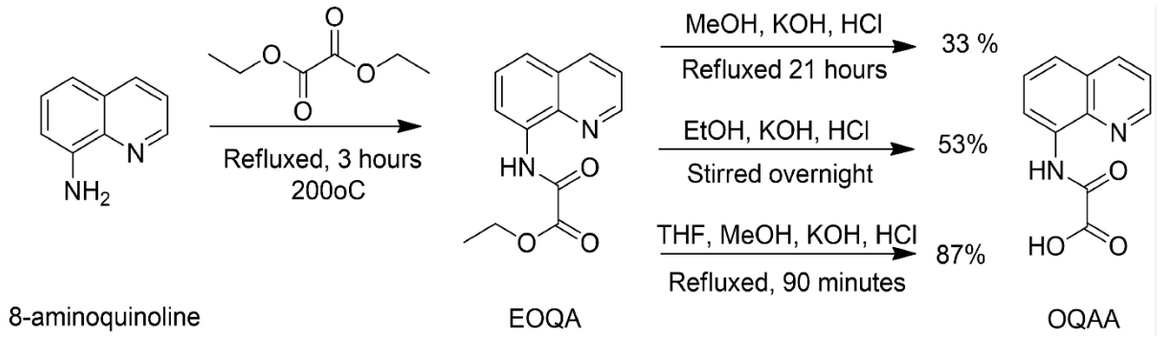

FIGURE 1. Structure and synthetic route on synthesis derivatives of 8-amidoquinoline

unviewable in deuterated protic solvents. A protic solvent like $(CD_3)_2SO$ is capable of hydrogen bonding, and such labile proton usually would exchange between H and D rapidly (Williams & Fleming 2007). Therefore, proton signals from O-H of acid or N-H of amide from OQAA do not show up. Assuming a peak at 11.1 ppm among O-H or N-H, we confirmed that peak was N-H. To deduce N-H due to ppm for N-H amide for EOQ almost at a similar peak of 11.3 ppm.

Though elucidation of OQAA can be confirmed based on the calculated number of carbon peaks present in ^{13}C NMR of OQAA as predicted (11 C), whereas the calculated number of carbon peaks present in ^{13}C NMR of EOQA (13C). The loss of the functional group of ethyl ($-CH_2CH_3$) made the ^{13}C NMR spectra of OQAA loss of 2 carbons from ^{13}C NMR spectra of EOQA (Figure 2(b)).

As for FTIR-ATR analysis, the formation for both parent compounds was confirmed by the appearance of the carbonyl group (C=O) stretching at 1699.7 cm^{-1} and 1688.5 cm^{-1}, alkene group from quinoline ring (C=C stretch) at 1528.2 cm^{-1} and 1498.4 cm^{-1}, and appearance of the secondary amide group (O=C-NH, s) at 3306.1 cm^{-1} and 3448.8 cm^{-1} in FTIR spectra of EOQA and OQAA respectively. The N-H stretching modes of antisymmetric aromatic are observed at ~3450 cm^{-1} (Nandiyanto, Oktiani & Ragadhita 2019; Ozel, Celik & Akyuz 2009). The addition of a single and broad OH group at 3242 cm^{-1} proved the successful reduction of EOQA to OQAA (Supplementary Materials).

A positive mode of direct infuse of ESI-MS corroborates the formation of EOQA and OQAA compounds. The ESI-MS results were compared with relative molecular mass (RMM) for the respective EOQA [$C_{13}H_{12}N_2O_3$], and OQAA [$C_{11}H_8N_2O_3$] is 244.2460 g/mol and 216.1928 g/mol (Supplementary Materials). According to the ESI-MS peaks, the mass divided by charge number (m/z) obtained for EOQ and OQAA were 267.0749 and 217.0600 a.m.u, respectively. The m/z values demonstrated sodium adduct $[M+Na]^+$ formation for EOQ while protonated molecule $[M+H]^+$ was detected in OQAA. Na^+ ion exists due to glassware, instruments, and/or impurity in solvents or chemicals used during sample preparation (Mortier et al. 2004). These characterizing and explanation results demonstrated that both compounds, especially OQAA, were successfully synthesized.

SCREENING OF OQAA WITH METAL IONS UNDER LONG WAVELENGTH OF UV'S LAMP

The fluorescence changes of mixtures of OQAA and metal salts were observed and recorded under a long wavelength of UV's lamp (Figure 3). OQAA solution was fluoresced by itself under the longwave UV lamp. However, once OQAA solutions were mixed with Fe^{2+}, Cu^{2+}, Co^{2+}, or Ni^{2+}, the fluorescence of OQAA was completely turned off. Meanwhile, the fluorescence intensity of the mixture of OQAA and Hg^{2+} or Cd^{2+} were slightly quenched. The fluorescence of OQAA-Zn^{2+} was enhanced remarkably upon the binding. The enhancement of the fluorescence intensity is attributed to the electron transfer from OQAA (electron donor) to the metal Zn^{2+} in forming complex (electron acceptor) (Sahudin et al. 2019). Therefore, Figure 3 showed that OQAA could be used as Zn^{2+},s label qualitatively under a long wavelength of UV's lamp due to remarkable fluorescent colour changes seen upon mixing with Zn^{2+} solution.

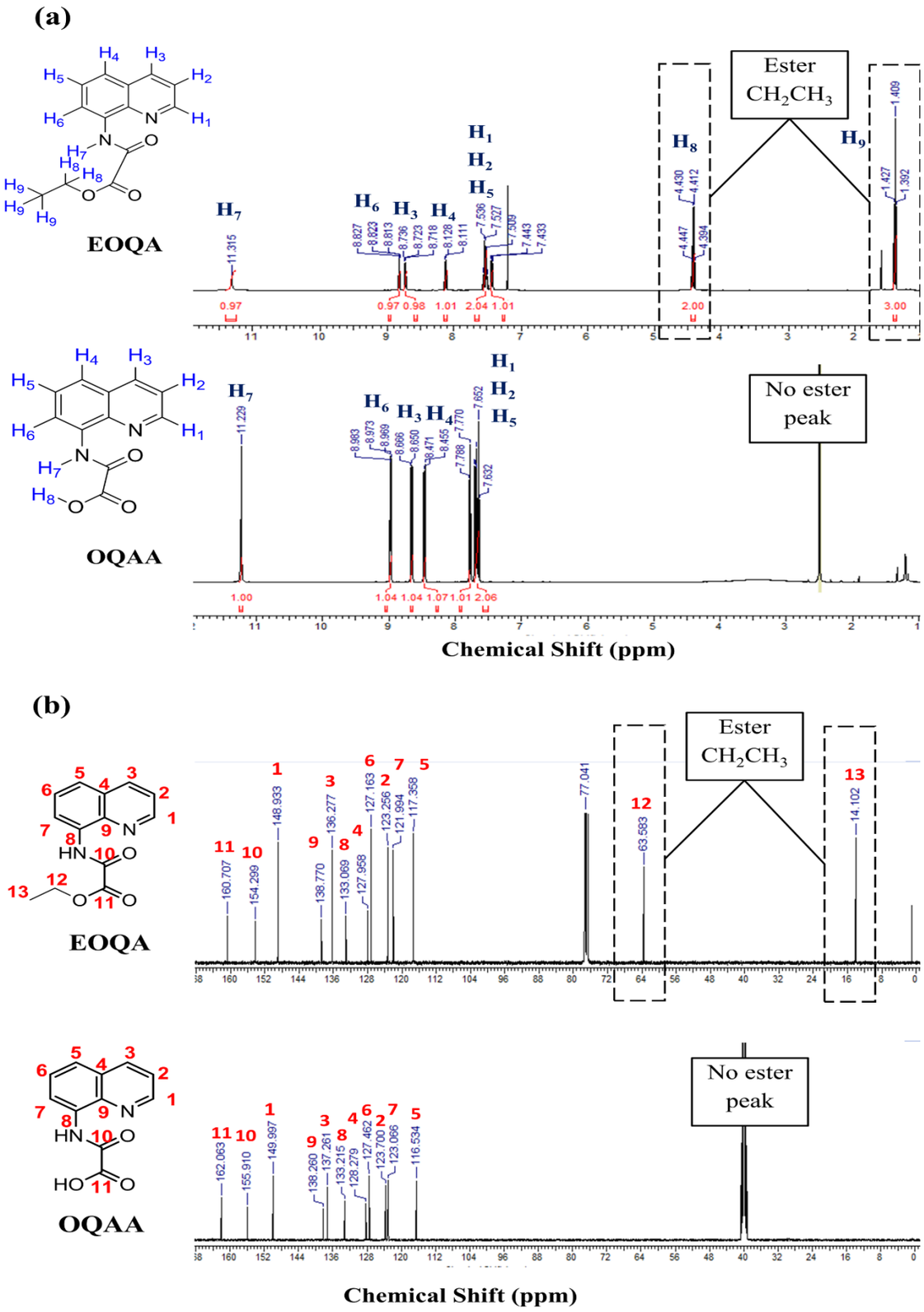

FIGURE 2. Comparison of (a) ^{1}H-NMR's spectra of EOQA and OQAA, and (b) ^{13}C-NMR's spectra of EOQA and OQAA

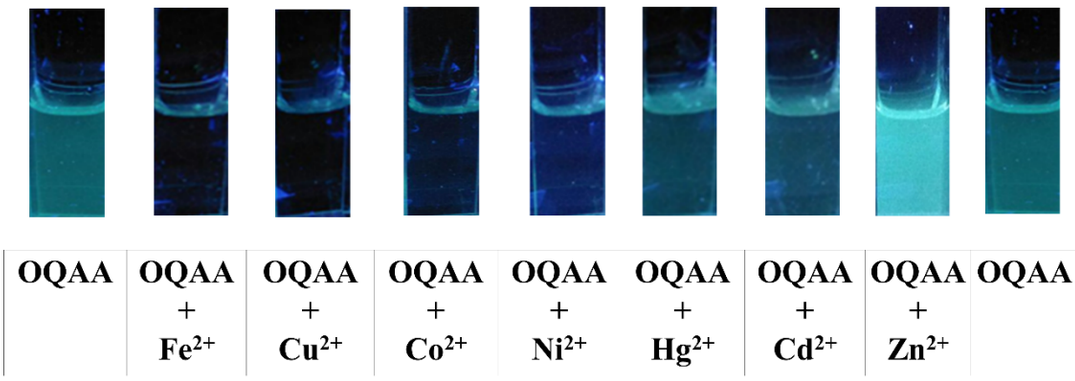

FIGURE 3. The fluoresce of OQAA and the fluorescence intensity changes of OQAA (1 mM) with metal salts (1 mM) of $Cd(NO_3)_2{\cdot}4H_2O$, $Co(NO_3)_2{\cdot}6H_2O$, $CuSO_4{\cdot}5H_2O$, $NiCl_2{\cdot}6H_2O$, $FeSO_4{\cdot}7H_2O$, $HgCl_2$, and $(Zn(SO_4){\cdot}7H_2O)$ under the long wavelength of UV's lamp (365 nm)

FLUORESCENCE AND ABSORPTION SPECTRAL RESPONSES TOWARDS VARIOUS METAL CATIONS

The influence of water content on the fluorescence of the OQAA was firstly investigated. Figure 4(a) shows that the OQAA emitted different wavelengths at different water ratios in the DMSO solvent. After adding water content into OQAA's solution, fluorescence intensity was quenched continuously, accompanied by a blue shift of the emission peak from 456 nm to 407 nm. These findings showed that the shift occurred at a distance of 49 nm between 50% and 100% water. Figure 4(b) shows that increasing the water content from 50% to 55%, 60%, 65%, and 70% resulted in longer emission wavelengths. The wavelengths were 456 nm to 476 nm, 470.5 nm, 463.5 nm, and 462.5 nm. The wavelength then shifted dramatically to a lower wavelength drastically changed and shifted to a shorter wavelength at 80% (417.5 nm) and then slowly shifted to 407 nm as the water content increased to 85%, 90%, 95%, and 100%. Even though 50% water content had a lower wavelength than some other water content, it demonstrated the most significant increase in fluorescence intensity. Thus, a binary solvent of 50% water and 50% DMSO was utilized to get optimum results.

JOB'S PLOT ANALYSIS OF OQAA AND ZN(II) VIA FLUORESCENCE SPECTROSCOPY

The stoichiometric ratio between OQAA and Zn^{2+} was done by a continuous variation method known as Job's plot. In this method, stock solutions of the same concentration of 10 µM OQAA and Zn^{2+} were prepared. Then the plot was drawn by plotting the fluorescence titration of complexometric OQAA- Zn^{2+} in command ratio (0 to 1). The maximal fluorescence intensity emitted at an approximately 0.5-mole ratio of Zn^{2+}, indicating the chelate complex of OQAA-$Zn^{2+,}$ has 1:1 stoichiometry (M_1L_1) (Figure 4(c).

BINDING STUDIES BETWEEN OQAA AND ZN(II) USING 1H-NMR SPECTROSCOPY

The NMR spectroscopic method can also provide practical information on binding studies between two reactants, like the interaction of OQAA as ligand towards Zn(II) ion (Nitsche & Otting 2018). Based on Figure 5, the presence of Zn^{2+} resulted in deshielding hydrogen's peak of N-H amide and proton's signal of quinoline moieties towards downfield (higher chemical shift). After adding one equivalent of Zn^{2+} to the solution of OQAA in $(CD_3)_2SO$, the proton's signal from N-H amide moves more to the downfield region from 11.1 ppm to 11.3 ppm. As the equivalent of Zn^{2+} increases, the proton's peak gradually increases until 11.4 ppm. This substantial movement of amide N-H hydrogen to a higher chemical shift implies that Zn^{2+} is binding to an amide. Other than that, the intensity of the proton signals of N-H amide decreases abruptly after OQAA is mixed with Zn^{2+} solution. As seen in the spectra, the other peaks (quinoline) also showed slight changes to downfield upon the binding with Zn(II).

However, the quinoline protons peak of OQAA does not shift downfield though the ratio of Zn^{2+} was

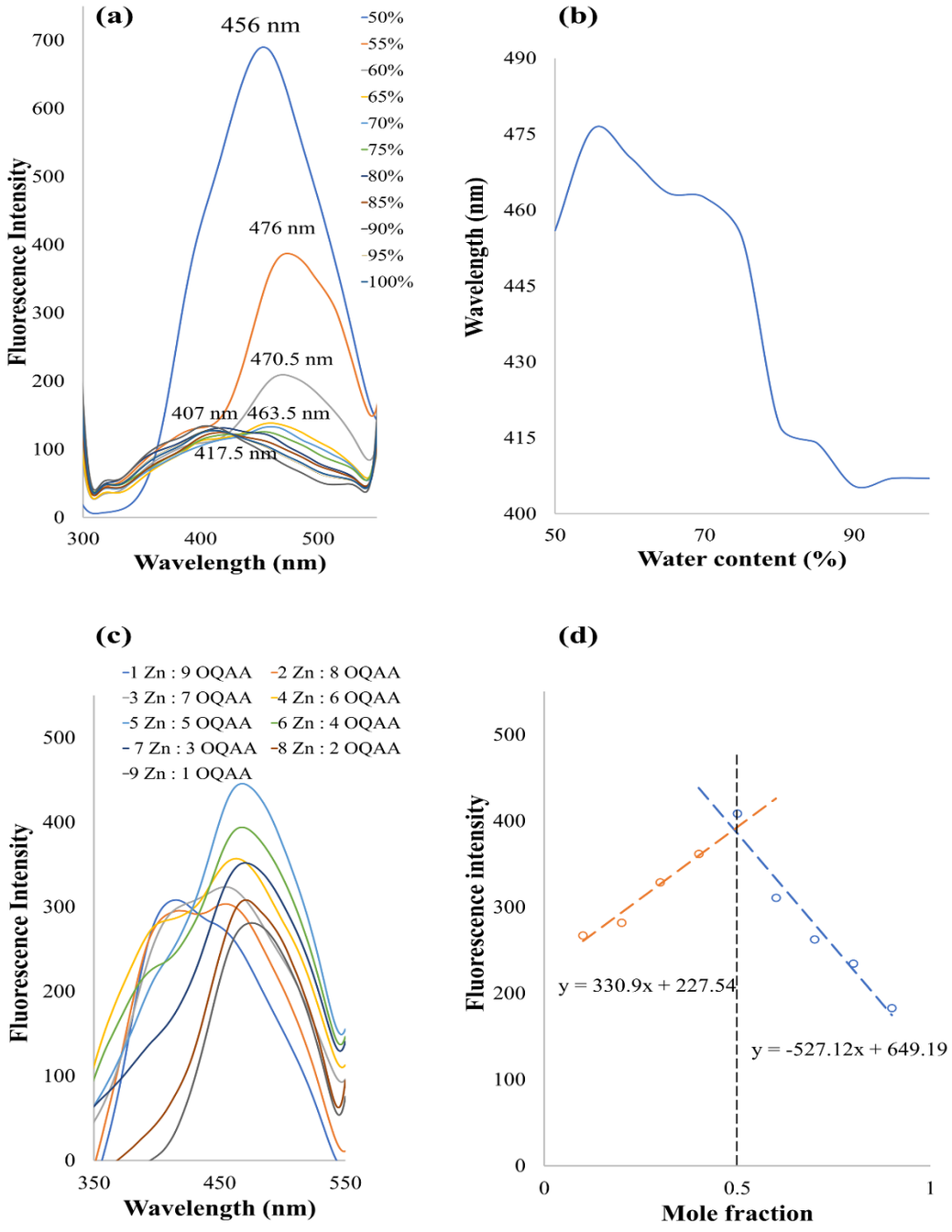

FIGURE 4. (a) The fluorescence spectra of OQAA at a concentration of 3×10^{-4} M in DMSO solution in the presence of various water ratios (50-100%); (b) The changes of emission's wavelength of OQAA upon changes the water content. Determining the binding ratio of OQAA-Zn by using the equimolar stock of OQAA and Zn (SO4)·$7H_2O$ at a concentration of 3×10^{-4} M. (c) Fluorescence spectra of continuous variation titration, and (d) Job's plot of OQAA and Zn^{2+} at wavelength 490 nm

increased up to four equivalents. This observation implies that nitrogen in quinoline does not bind to Zn^{2+} or might have slight interactions with Zn^{2+} than the N-H peak of amide. These changes were also evident in Song and Zhang (2019)'s findings. Their N-H proton at 11.3 ppm is gradually absent upon increasing an equivalent stock solution of Zn^{2+} ion (0 - 1.0 eq.) while the other slightly shifted peaks. As in Mehdi et al. (2017)'s study, the N-H peak of amide just shifted from 11.9 to 11.97 ppm without any changes on the intensity peak, and quinoline peaks shifted and broadened slightly. They considered the coordination of Zn were O-atom of amide and N-atom of quinoline molecules of probe OQAA.

Therefore, the changes of the proton's peaks of amide and quinoline demonstrated interactions among the ligand OQAA (possibly N-atom or O-atom of amide and N-atom of quinoline) metal Zn^{2+} ion. Further addition of Zn^{2+} of more than the 1:1 ratio did not lead to any further remarkable changes in the chemical shifting, which proved the metal-ligand binding at 1:1 stoichiometry. This result supports Job's plot analysis experiment.

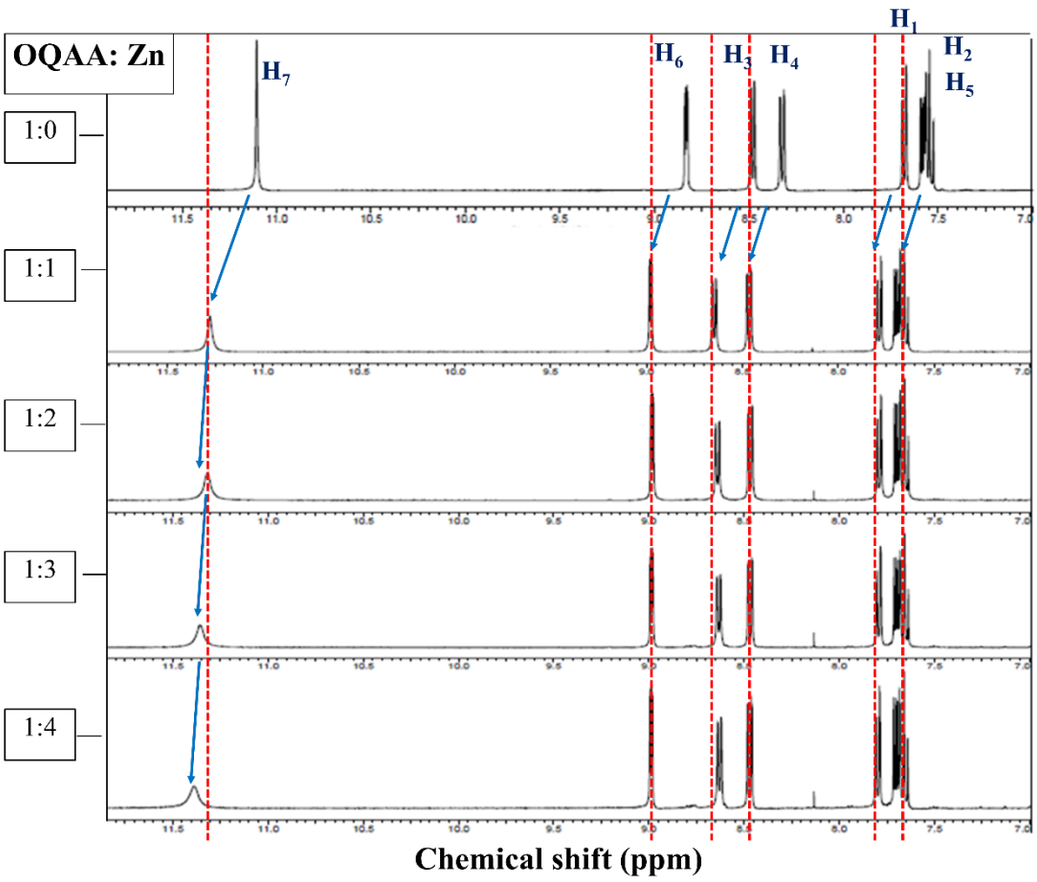

FIGURE 5. ^{1}H NMR titration to form OQAA-Zn in solution beginning from a solution of OQAA until the ratio at 1 OQAA: 4 Zn^{2+}

OPTIMIZED MOLECULAR STRUCTURE OF OQAA USING DFT

In the domains of chemical, biological, and material sciences, computational chemistry is becoming increasingly relevant. It has produced almost precise structural insights into synthetic and natural products (Hashmi et al. 2014). It also aids in the knowledge of molecular structure in organic chemistry, providing insight into reaction pathways and chemical reactions by assessing geometrical features of molecules (Kerru et al. 2019). The electronic and geometrical properties

are computed using Density Functional Theory (DFT), significantly improving organic and inorganic synthesis. Therefore, the optimized geometry of OQAA was obtained by performing the B3LYP/6-31G(d, p) level of theory, and the scan of the potential energy surface (PES) was at the lowest amount of energy (Total Energy = -1.99 × 10^6 kJ/mol) (Figure 6(a)). The OQAA's theoretical geometry of type of bond, bond length (BL) in Å and bond angle (BA) in º were presented in Table 1. Aside from the ring structure of quinoline, an aromatic bond is also denoted in N24-C16 due to electron delocalization between three atoms, including O17. The BA of the oxygen atom of oxoacid is almost similar to the fixed atoms C16 and C18. C16-C18-O17, C16-C18-O19, C16-C18-O20, and O19-C18-O20 recorded 118.86273, 123.73535, 111.79952, and 124.07349, respectively. Thus, this optimized algorithm structure was used for the subsequent calculation theories.

TABLE 1. Comparison between theoretical and experimental NMR chemical shifts (^{1}H and ^{13}C) for OQAA

Number of atoms	^{1}H NMR			^{13}C NMR		
	Theoretical (ppm)	Experimental (ppm)	Percentage difference (%)	Theoretical (ppm)	Experimental (ppm)	Percentage difference (%)
1	N/A	N/A	N/A	107.14	123.1	12.97
2	N/A	N/A	N/A	123.76	133.2	7.09
3	N/A	N/A	N/A	127.66	138.3	7.69
4	N/A	N/A	N/A	115.86	128.3	9.70
5	N/A	N/A	N/A	111.65	116.5	4.16
6	N/A	N/A	N/A	113.33	127.5	11.11
7	7.77	8.85, dd, J = 1.6, 4.0 Hz	12.20	N/A	N/A	N/A
8	N/A	N/A	N/A	123.51	137.3	10.04
9	8.00	8.99, dd, J = 1.6, 8.0 Hz	11.01	N/A	N/A	N/A
10	8.00	7.71, m	N/A	N/A	N/A	N/A
11	N/A	N/A	N/A	108.28	123.7	12.47
12	N/A	N/A	N/A	133.91	149.9	10.67
13	8.5	8.68, dd, J = 1.2, 7.6 Hz	2.07	N/A	N/A	N/A
14	7.77	7.71, m	0.78	N/A	N/A	N/A
15	9.04	7.79, dd, J = 1.2, 8.0 Hz	16.05	N/A	N/A	N/A
16	N/A	N/A	N/A	145.05	155.9	6.96
17	N/A	N/A	N/A	N/A	N/A	N/A
18	N/A	N/A	N/A	144.16	162.1	11.07
21	6.04	-	N/A	N/A	N/A	N/A
22	10.58	11.10	4.68	N/A	N/A	N/A

Experimental value was taken from Figure 2, and Number of atoms based on optimized geometry of OQAA from Figure 6

^{1}H NMR and ^{13}C NMR ANALYSIS OF OQAA

NMR plays a crucial role in elucidating known and unknown molecular structures by providing information on 1D (^{1}H and ^{13}C) and 2D (homonuclear and heteronuclear) (Bányai 2018). ^{1}H NMR and ^{13}C NMR of OQAA were measured in deuterated DMSO on a 400 MHz spectrometer with TMS as a standard reference. Computational NMR for both H and C elements was calculated using DFT/B3LYP/6-31G (d,p)/Gauge-Independent Atomic Orbital (GIAO) gaseous phase with TMS as reference. Table 2 compares theoretical and experimental NMR of H and C. As shown in Table 2, the correlation chemical shift between theoretical and experimental can be considered agreeably since the percent difference for both NMR was calculated below 16% (Oturak, Kinaytürk & Sahin 2015). This is because the experimental and DFT environments for NMR analysis are very different. The experimental molecule was run in DMSO solvent, whereas the DFT molecule was run in the gas phase. Besides, OH's calculation peak can be easily observed while the experimental peak was absent due to its exchangeability between H and D, as mentioned before.

TABLE 2. Comparison between theoretical and experimental IR analysis of OQAA and their assignments

Assignment	Theoretical	Experimental	Percentage difference (%)
C=C aromatic, w	1794	1502	19.44
C=O,s	1866	1688	10.55
C-H stretch,s	3170	3078	2.99
O.H., s, b	3209	3242	1.02
N-H 2º amide, s	3587	3492	2.72

Experimental value was taken from Supplementary

FREQUENCIES ANALYSIS OF OQAA

The essential techniques for confirming chemical elements that make up the compound and identifying the modes of vibrations are spectroscopic analysis (FTIR). Therefore, the superposition and assignment of each vibrational analysis, theoretical and experimental, were summarized in Table 2. The C=C aromatic peak had the most significant difference, at 19.44%. Theoretical values (1794 cm^{-1}) are greater than experimental values (1502 cm^{-1}). This discrepancy can be explained because the DFT calculations were performed on a single molecule and gas phase. The remaining functional groups, C=O (10.55%), C-H stretch (2.99%), OH (1.02%), and secondary amide, N-H (2.72 %), showed a modest percentage of divergence. Since there is not much discrepancy between the two data sets, they were in fair agreement.

TABLE 3. Calculated wavelengths, excitation energy, and oscillator strength of OQAA at DFT/B3LYP/6-31G (d,p)/TD-DFT

	Wavelegth (nm)	Excitation energy (eV)	Oscillator Strength
1	320.65	4.3567	0.0996
2	288.10	4.3736	0.0009
3	283.03	4.3807	0.0066
4	282.30	4.3920	0.0005
5	272.76	4.5455	0.0291
6	261.04	4.7496	0.0257
7	237.85	5.2128	0.0080

UV-Vis ANALYSIS OF OQAA

The theoretical TD-DFT and experimental UV–Vis absorption spectra of OQAA are visualized in Supplementary Materials. A reasonably close consensus has been shown between the observed and the simulated spectra. Time-dependent functional theory (TD-DFT) at the B3LYP/6- 31G (d,p) level of theory in the gas phase was used to simulate the UV-Vis spectra of the optimized structure at the ground state. This simulated UV-Vis was calculated by measuring the electronic transition's probability using oscillator strength (f). Calculated wavelengths, excitation energy, and oscillator strength of OQAA at DFT/B3LYP/6-31G(d,p)/TD-DFT were recorded in Table 3. The higher and maximum absorbance was noted. As for OQAA, both results showed two absorption bands. The absorption band of 257 nm (theory) and 267 nm (experiment) may be attributed to the $n \rightarrow \pi^*$ transition of carbonyl (C=O), while the highest and strongest absorption band of 328 nm (theory) and 320 nm (experiment) showed an electronic transition from $\pi \rightarrow \pi^*$ transition of aromatic chromophores (Supplementary Materials). The gap between theoretical and experimental values for the $n \rightarrow \pi^*$ transition was 10 nm, whereas the difference for the $\pi \rightarrow \pi^*$ transition was 8 nm.

MOLECULAR ELECTROSTATIC SURFACE POTENTIAL

Molecular electrostatic potential (MEP) is a highly effective method for determining or predicting the reactive regions of possible nucleophilic and electrophilic attacks on the compound. In other words, by predicting electrophilic and nucleophilic in the investigated compound, the reactivity of the title compound can be explained (Szabó et al. 2009). MEP helps illustrate the potential of positive charge at any point in the molecule's space, indicating total charge electron density distribution (Prabavathi, Nilufer & Krishnakumar 2014). As shown in Figure 6(b), this potential decrease from positive site (7.208E-2 a.u) to negative site (-7.208E-2 a.u) in the following colour order (blue> green> yellow> orange>red).

The OQAA's total isoelectronic density mapped surface, nucleophilic reactivity localized on the oxygen atoms of amide (-0.0392 a.u) and carboxylic acid (-0.0343 a.u). However, another oxygen atom of the acid covered in the blue region with the OQAA molecule showed a positive mapped value of 0.0279 a.u. Besides that, N-atom in the pyridine ring also showed a similar value of 0.0295 a.u. A nitrogen atom of aminoquinoline showed electrostatic potential close to zero and virtual in green colour. This region of close to zero potential is the same as the π-system in the aromatic ring of OQAA, which illustrates the electrophilic region.

Presumably, the interaction site for Zn complexation will most likely be negatively charged, covering the C=O of the amide and acid. None of the N-atom probable involved upon binding with Zn. These may be due to negative charge covers; both O-atoms have been assumed more 'harder' than neutral N-atom (Atalay, Di Toro & Carbonaro 2013; Chandrakumar & Pal 2002). Generally based on Pearson's Hard–Soft Acid-Base (HSAB) theory, the preference for good Lewis acid of Zn^{2+} will bind to the hard Lewis base of the donor atom of oxygen (Awual et al. 2013; Mancin & Tecilla 2007).

FRONTIER MOLECULAR ORBITAL ANALYSIS OF OQAA

One of the two pivotal molecular orbitals is the highest occupied molecular orbital (HOMO), which depicts the most distant molecular orbital filled with electrons and works as an electron donor. The other is the lowest unoccupied molecular orbital (LUMO), representing an electron acceptor in the inmost molecular orbital. Both of these molecular orbitals were called frontier molecular orbitals. Essentially, the energy gap values between HOMO and LUMO provide a valuable tool for determining a molecule's electronic transition, optical characteristics, kinetic stability, and chemical reactivity (Salim et al. 2018).

The smaller the energy gap values, the more stable and reactive the molecule is because they can be stimulated by small energies, resulting in the HOMO that could move quickly into the LUMO. Hence, the determination of HOMO-LUMO energy gap values is essential in describing the chemical behavior and electronic properties of OQAA. The energy band's gap of OQAA as features in Figure 6(c) was calculated to be 0.1124 eV. This gap's value was much lower than the zinc's fluorophore reported by Hudson et al. (2010) that using the similar basis set as OQAA (6-31G(d,p)), the energy gap of that fluorophore (anthracen-9-yl)-N, N dimethylmethanamine was recorded at 3.52 eV while methylpyridine 6.23 eV. As Probe L reported by Sethupathi et al. (2020), the energy gap was calculated to be 2.48 eV. Due to the narrower energy gaps, OQAA was more reactive than those probes employed in zinc detection.

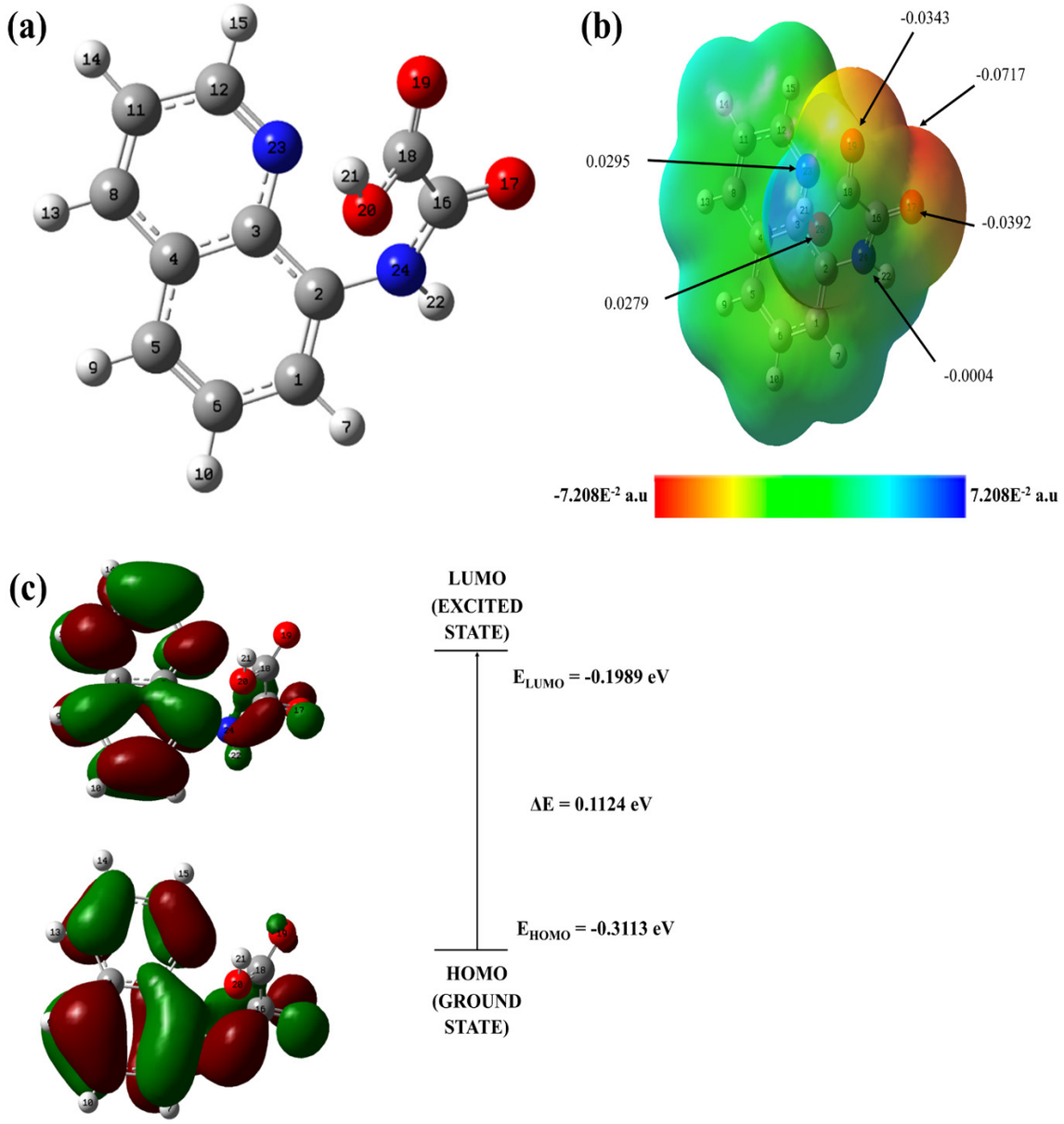

FIGURE 6. (a) The atom numbering scheme implemented in the optimized molecular geometry of OQAA at B3LYP/6-31G(d, p) level of theory. Dark grey, light grey, red and blue spheres refer to C, H, O, and N (Total Energy = -1.99 × 10^6 kJ/mol), (b) Determination of electrophilic and nucleophilic reaction based on total electron density mapped with the molecular electrostatic potential of OQAA, and (c) The atomic orbital composition of HOMO and LUMO of OQAA at isovalue 0.02, calculated at frontier molecular orbital using DFT/B3LYP/6-31G (d,p)

CALCULATION OF OQAA-ZN COMPLEX

The total energy of OQAA-Zn in optimized geometry using DFT/B3LYP/GEN/LANL2DZ was -2.165 × 10^6 kJ/mol (Supplementary Materials). Meanwhile, BSSE energy using the CP approach was calculated at -1.722. × 10^5 kJ/mol. As per Equation (1), the corrected interaction energy between the OQAA-Zn complex was calculated -2.337 × 10^6 kJ/mol. This energy value showed that the

energy of OQAA-Zn was decreasing from the energy of ligand OQAA (-1.99 × 10^6 kJ/mol), thus indicating the interaction between OQAA-Zn was highly strong and stable (Kaur, Chhibber & Mittal 2017; Ying et al. 2019).

Conclusion

OQAA investigated as a Zn^{2+} probe has been successfully synthesized and characterized using NMR (^1H and ^{13}C), FT-IR, UV-Vis, and ESI-MS spectroscopic techniques. From these, the excitation energy of OQAA was found at wavelength 320 nm, as same as the experimental wavelength of absorption of OQAA using DMSO as solvent. As discussed, other theoretical calculations also almost showed a similar result to the experimental one. Due to the vivid fluorescent colour changes observed upon mixing with Zn^{2+} solution, the preliminary binding screening demonstrated that OQAA might be employed as Zn^{2+},s label qualitatively at a long wavelength of UV light. Using Job's plot and ^1H NMR titration methods showed that the binding behavior of compound OQAA towards Zn^{2+} afforded a complexation with a 1:1 binding ratio. The calculated interaction energy showed that the binding between ligand OQAA and metal Zn was strong and stable. Thus, future research will explore OQAA in developing a Zn^{2+} fluorescent sensor used in environmental and biological applications.

Acknowledgements

The authors would like to extend their utmost gratitude for the financial support (GUP-2016-059) and facilities provided by Universiti Kebangsaan Malaysia. We would also like to express our gratitude to the Center for Information and Communication Technology (CICT), UTM, under the Fundamental Research Grant Scheme (FRGS, Vot R.J130000.7854.5F471), for supporting and providing facilities and services of high-performance computing to reduce the investigation time.

References

Al-Khalqi, E.M., Hamid, M.A.A., Shamsudin, R., Al-Hardan, N.H., Jalar, A. & Keng, L.K. 2021. Zinc oxide nanorod electrolyte-insulator- Semiconductor sensor for enhanced 2-Methoxyethanol selectivity. *IEEE Sensors Journal* 21(5): 6234-6240.

Atalay, Y.B., Di Toro, D.M. & Carbonaro, R.F. 2013. Estimation of stability constants for metal-ligand complexes containing neutral nitrogen donor atoms with applications to natural organic matter. *Geochimica et Cosmochimica Acta* 122: 464-477.

Awual, M.R., Kobayashi, T., Miyazaki, Y., Motokawa, R., Shiwaku, H., Suzuki, S., Okamoto, Y. & Yaita, T. 2013. Selective lanthanide sorption and mechanism using novel hybrid Lewis base (N-Methyl-N-phenyl-1,10-phenanthroline-2-carboxamide) ligand modified adsorbent. *Journal of Hazardous Materials* 252-253: 313-320.

Bányai, I. 2018. Dynamic NMR for coordination chemistry. *The Royal Society of Chemistry* 42: 7569-7581.

Basabe-Desmonts, L., Müller, T.J.J. & Crego-Calama, M. 2007. Design of fluorescent materials for chemical sensing. *Chemical Society Reviews* 36(6): 993-1017.

Bozym, R.A., Thompson, R.B. & Fierke, C.A. 2006. Importance of measuring free zinc in cells. In *Reviews in Fluorescence 2006,* edited by Geddes, C.D. & Lakowicz, J.R. Boston: Springer. pp. 399-419.

Bukheet Hassan, H. 2014. Density function theory B3LYP/6-31G**calculation of geometry optimization and energies of donor-bridge-acceptor molecular system. *Research Article International Journal of Current Engineering and Technology* 4(4): 2342-2345.

Chandrakumar, K.R.S. & Pal, S. 2002. A systematic study on the reactivity of Lewis acid-base complexes through the local hard-soft acid-base principle. *Journal of Physical Chemistry A* 106(48): 11775-11781.

Chen, Y., Han, K.Y. & Liu, Y. 2007. Effective switch-on fluorescence sensing of zinc (II) ion by 8-Aminoquinolino-β-Cyclodextrin/Adamantaneacetic acid system in water. *Bioorganic and Medicinal Chemistry* 15(13): 4537-4542.

Czaplinska, B., Spaczynska, E. & Musiol, R. 2018. Quinoline fluorescent probes for zinc - from diagnostic to therapeutic molecules in treating neurodegenerative diseases. *Medicinal Chemistry* 14(1): 19-33.

Dong, Y., Fan, R., Chen, W., Wang, P. & Yang, Y. 2017. A simple quinolone schiff-base containing CHEF based fluorescence' turn-on' chemosensor for distinguishing Zn^{2+} and Hg^{2+} with high sensitivity, selectivity and reversibility. *Dalton Transactions* 46(20): 6769-6775.

Dong, Z., Le, X., Zhou, P., Dong, C. & Ma, J. 2014. An 'off-on-off' fluorescent probe for the sequential detection of Zn^{2+} and hydrogen sulfide in aqueous solution. *New Journal of Chemistry* 38(4): 1802-1808.

Fu, H., Liu, H., Zhao, L., Xiao, B., Fan, T. & Jiang, Y. 2019. A quinoline-based selective 'turn on' chemosensor for zinc (II) via Quad-core complex, and its application in live cell imaging. *Tetrahedron* 75(49): 130710.

Galano, A. & Alvarez-Idaboy, J.R. 2006. A new approach to counterpoise correction to BSSE. *Journal of Computational Chemistry* 27(11): 1203-1210.

Gupta, V.K., Jain, A.K. & Maheshwari, G. 2006. A new Zn^{2+}-selective potentiometric sensor based on dithizone - PVC membrane. *Chemia Analityczna* 51(6): 889-898.

Hashmi, M.A., Khan, A., Ayub, K. & Farooq, U. 2014. Spectroscopic and density functional theory studies of 5, 7, 3', 5'-Tetrahydroxyflavanone from the leaves of *Olea ferruginea*. *Spectrochimica Acta Part A: Molecular and Biomolecular Spectroscopy* 128: 225-230.

Hudson, G.A., Cheng, L., Yu, J., Yan, Y., Dyer, D.J., McCarroll, M.E. & Wang, L. 2010. Computational studies on response and binding selectivity of fluorescence sensors. *J. Phys. Chem. B* 114(2): 870-876.

Jensen, F. 2010. An atomic counterpoise method for estimating inter- and intramolecular basis set superposition errors. *Journal of Chemical Theory and Computation* 6(1): 100-106.

Kadir, M.A., Abdul Razak, F.I. & Haris, N.S.H. 2020. Experimental and DFT data of *p*-Chlorocalix[4]arene as drugs receptor. *Data in Brief* 32: 106263.

Siti Shafura, A.Karim, Chang-Fu Dee, Burhanuddin Yeop Majlis & Mohd Ambri Mohamed. 2019. Recent progress on fabrication of zinc oxide nanorod-based field effect transistor biosensors. *Sains Malaysiana* 48(6): 1301-1310.

Kaur, H., Chhibber, M. & Mittal, S. 2017. Acyclic arylamine-based ionophores as potentiometric sensors for Zn^{2+} and Ni^{2+} ions. *Journal of Carbon Research* 3(4): 34.

Kerru, N., Gummidi, L., Bhaskaruni, S.V.H.S., Maddila, S.N., Singh, P. & Jonnalagadda, S.B. 2019. A comparison between observed and DFT calculations on structure of 5-(4-chlorophenyl)-2-amino-1,3,4-thiadiazole. *Scientific Reports* 9(1): 1-17.

Khairul, Wan M., Mohd Faizuddin Abu Hasan, Adibah Izzati Daud, Hafiza Mohamed Zuki, Ku Halim Ku Bulat & Maisara Abdul Kadir. 2016. Theoretical and experimental investigation of pyridyl-thiourea derivatives as ionophores for Cu (II) ion detection. *Malaysian Journal of Analytical Sciences* 20(1): 73-84.

Li, Q.F., Wang, J.T., Wu, S., Ge, G.W., Huang, J., Wang, Z., Yang, P. & Lin, J. 2018. A water-soluble fluorescent chemosensor having a high affinity and sensitivity for Zn^{2+} and its biological application. *Sensors and Actuators, B: Chemical* 259: 484-491.

Lopes, J.F., Rocha, W.R., dos Santos, H.F. & de Almeida. W.B. 2010. An investigation of the BSSE effect on the evaluation of *ab initio* interaction energies for cisplatin-water complexes. *Journal of the Brazilian Chemical Society* 21(5): 887-896.

Ma, Q.J., Zhang, X.B., Han, Z.X., Huang, B., Jiang, Q., Shen, G.L. & Yu, R.Q. 2011. A ratiometric fluorescent probe for zinc ions based on the quinoline fluorophore. *International Journal of Environmental Analytical Chemistry* 91(1): 74-86.

Mancin, F. & Tecilla, P. 2007. Zinc(II) complexes as hydrolytic catalysts of phosphate diester cleavage: From model substrates to nucleic acids. *New Journal of Chemistry* 31(6): 800-817.

Mehdi, H., Gong, W., Guo, H., Watkinson, M., Ma, H., Wajahat, A. & Ning, G. 2017. Aggregation-Induced emission (AIE) fluorophore exhibits a highly ratiometric fluorescent response to Zn^{2+} *in vitro* and in human liver cancer cells. *Chemistry - A European Journal* 23(53): 13067-13075.

Mohamad, N.S., Zakaria, N.H., Daud, N., Tan, L.L., Goh, C.T., Lee, Y.H. & Hassan, N.I. 2021. The role of 8-amidoquinoline derivatives as fluorescent probes for zinc ion determination. *Sensors* 21(1): 311.

Mortier, K.A., Zhang, G.F., van Peteghem, C.H. & Lambert, W.E. 2004. Adduct formation in quantitative bioanalysis: Effect of ionization conditions on paclitaxel. *Journal of the American Society for Mass Spectrometry* 15(4): 585-592.

Nandiyanto, A.B.D., Oktiani, R. & Ragadhita, R. 2019. How to read and interpret FTIR spectroscope of organic material. *Indonesian Journal of Science and Technology* 4(1): 97-118.

Nitsche, C. & Otting, G. 2018. NMR studies of ligand binding. *Current Opinion in Structural Biology* 48: 16-22.

Oturak, H., Kaya Kinaytürk, N. & Sahin, G. 2015. Structure and vibrational studies of ±1-(1H-benzoimidazol-2-YL) ethanol, using DFT method. *Acta Physica Polonica A* 128(2): 417-421.

Ozel, A.E., Celik, S. & Akyuz, S. 2009. Vibrational spectroscopic investigation of free and coordinated 5-aminoquinoline: The IR, Raman and DFT studies. *Journal of Molecular Structure* 924-926: 523-530.

Park, G.J., Kim, H., Lee, J.J., Kim, Y.S., Lee, S.Y., Lee, S., Noh, I. & Kim, C. 2015. A highly selective turn-on chemosensor capable of monitoring Zn^{2+} concentrations in living cells and aqueous solution. *Sensors and Actuators, B: Chemical* 215: 568-576.

Petyunin, G.P. & Sysun, V.N. 1974. Preparation of aminoacridine salts. *Pharmaceutical Chemistry Journal* 9(7): 444-447.

Ponnuvel, K. & Padmini, V. 2016. Turn-on fluorescence chemosensor for fluoride ions and its applicability in imaging of living cells. *Journal of Luminescence* 169: 289-294.

Prabavathi, N., Nilufer, A. & Krishnakumar, V. 2014. FT-IR, FT-Raman and DFT quantum chemical study on the molecular conformation, vibrational and electronic transitions of 1-(m-(Trifluoromethyl)phenyl) piperazine. *Spectrochimica Acta - Part A: Molecular and Biomolecular Spectroscopy* 121: 483-493.

Sahudin, M.A., Su'ait, M.S., Tan, L.L., Lee, Y.H. & Abd Karim. N.H. 2019. Zinc (II) salphen complex-based fluorescence optical sensor for biogenic amine detection. *Analytical and Bioanalytical Chemistry* 411(24): 6449-6461.

Salim, A.S., Girgis, A.S., Basta, A.H., El-Saied, H., Mohamed, M.A. & Bedair, A.H. 2018. Comparative DFT computational studies with experimental investigations for novel synthesized fluorescent pyrazoline derivatives. *Journal of Fluorescence* 28(4): 913-931.

Sethupathi, M., Jayamani, A., Muthusankar, G., Sakthivel, P., Sekar, K., Gandhi, S., Sengottuvelan, N., Gopu, G. & Selvaraju, C. 2020. Colorimetric and fluorescence sensing of Zn^{2+} ion and its bio-imaging applications based on macrocyclic "tet a" derivative. *Journal of Photochemistry and Photobiology B: Biology* 207: 111854.

Shamsipur, M., Yousefi, M., Hosseini, M., Ganjali, M.R., Sharghi, H. & Naeimi, H. 2001. A Schiff base complex of Zn (II) as a neutral carrier for highly selective PVC membrane sensors for the sulfate ion. *Analytical Chemistry* 73(13): 2869-2874.

Shi, D., Zhou, X. & Zheng, T. 2014. Recognition and fluorescent sensing of zinc ions using organic fluorophores-based sensor molecules. *Journal of the Iranian Chemical Society* 12(2): 293-308.

Shyamal, M., Mazumdar, P., Maity, S., Samanta, S., Sahoo, G.P. & Misra, A. 2016. Highly selective turn-on fluorogenic chemosensor for robust quantification of Zn (II) based on aggregation induced emission enhancement feature. *ACS Sensors* 1(6): 739-747.

Song, H. & Zhang, Z. 2019. A quinoline-based ratiometric fluorescent probe for discriminative detection of Zn^{2+} and Cd^{2+} with different binding modes, and its Zn^{2+} complex for relay sensing of pyrophosphate and adenosine triphosphate. *Dyes and Pigments* 165: 172-181.

Szabó, L., Chiş, V., Pîrnău, A., Leopold, N., Cozar, O. & Orosz, Sz. 2009. Spectroscopic and theoretical study of amlodipine besylate. *Journal of Molecular Structure* 924: 385-392.

Tharmaraj, V. & Pitchumani, K. 2013. A highly selective ratiometric fluorescent chemosensor for Cu(II) based on dansyl-functionalized thiol stabilized silver nanoparticles. *Journal of Materials Chemistry B* 1(14): 1962-1967.

Tian, X., Guo, X., Yu, F. & Jia, L. 2016. An oxalamidoquinoline-based fluorescent sensor for selective detection of Zn2+ in solution and living cells and its logic gate behavior. *Sensors and Actuators, B: Chemical* 232: 181-187.

Urano, Y., Kamiya, M., Kanda, K., Ueno, T., Hirose, K. & Nagano, T. 2005. Evolution of fluorescein as a platform for finely tunable fluorescence probes. *Journal of the American Chemical Society* 127(13): 4888-4894.

Williams, D. & Fleming, I. 2007. *Spectroscopic Methods in Organic Chemistry*. 6th ed. London: McGraw-Hill Education.

Ying, K.S., Awang Ngah, F.A., Sapari, S., Lee, Y.H. & Hasbullah, S.A. 2019. Complexation study of bis-thiourea compound with aluminium ion as ionophore for development of potentiometric ion sensor. *Sains Malaysiana* 48(12): 2649-2661.

You, Q.H., Chan, P.S., Chan, W.H., Hau, S.C.K., Lee, A.W.M., Mak, N.K., Mak, T.C.W. & Wong, R.N.S. 2012. A quinolinyl antipyrine based fluorescence sensor for Zn^{2+} and its application in bioimaging. *RSC Advances* 2(29): 11078-11083.

Yue, Y., Dong, Q., Zhang, Y., Sun, Y. & Gong, Y. 2015. A highly selective 'turn-on' fluorescent chemosensor based on 8-aminoquinoline for detection of Zn^{2+}. *Analytical Methods* 7(13): 5661-5666.

Zhang, Y., Guo, X., Si, W., Jia, L. & Qian, X. 2008. Ratiometric and water-soluble fluorescent zinc sensor of carboxamidoquinoline with an alkoxyethylamino chain as receptor. *Organic Letters* 10(3): 473-476.

*Corresponding author; email: drizz@ukm.edu.my

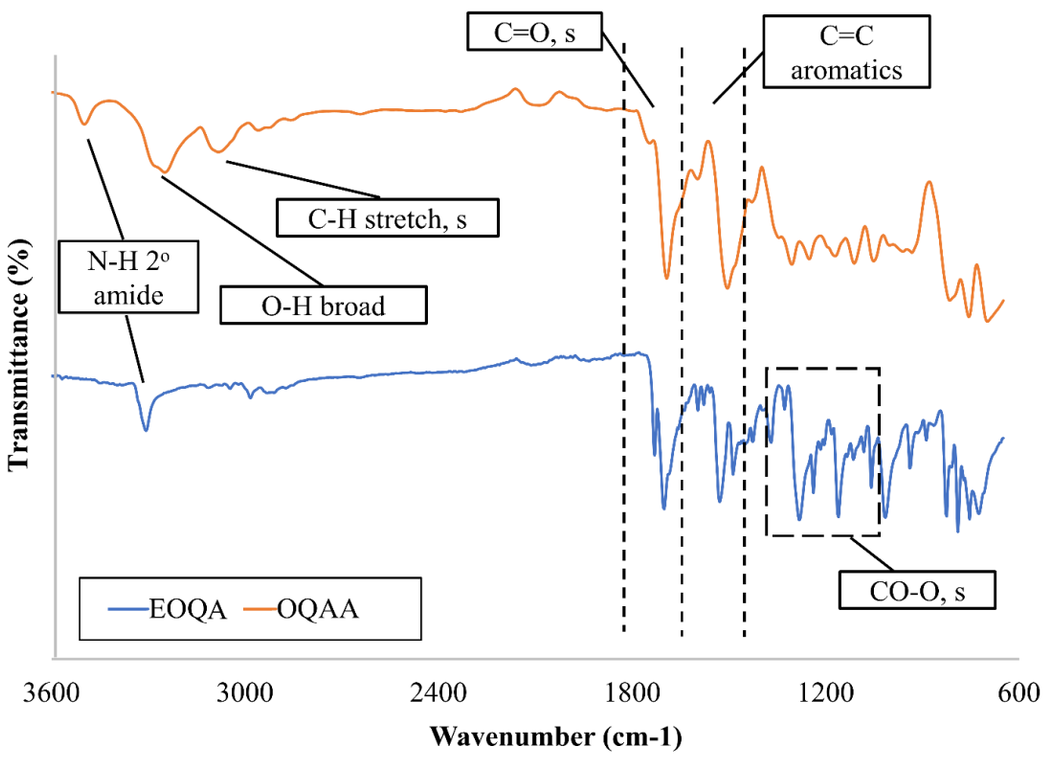

SUPPLEMENTARY 1. Comparison of FTIR's spectra of EOQA and OQAA

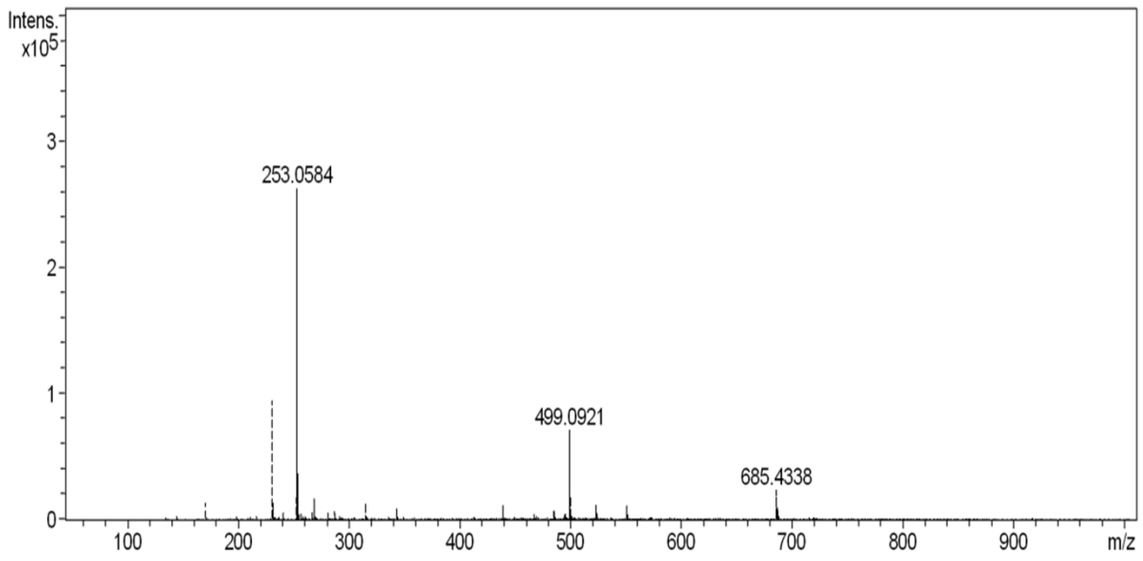

SUPPLEMENTARY 2. ESI-MS spectra of EOQA

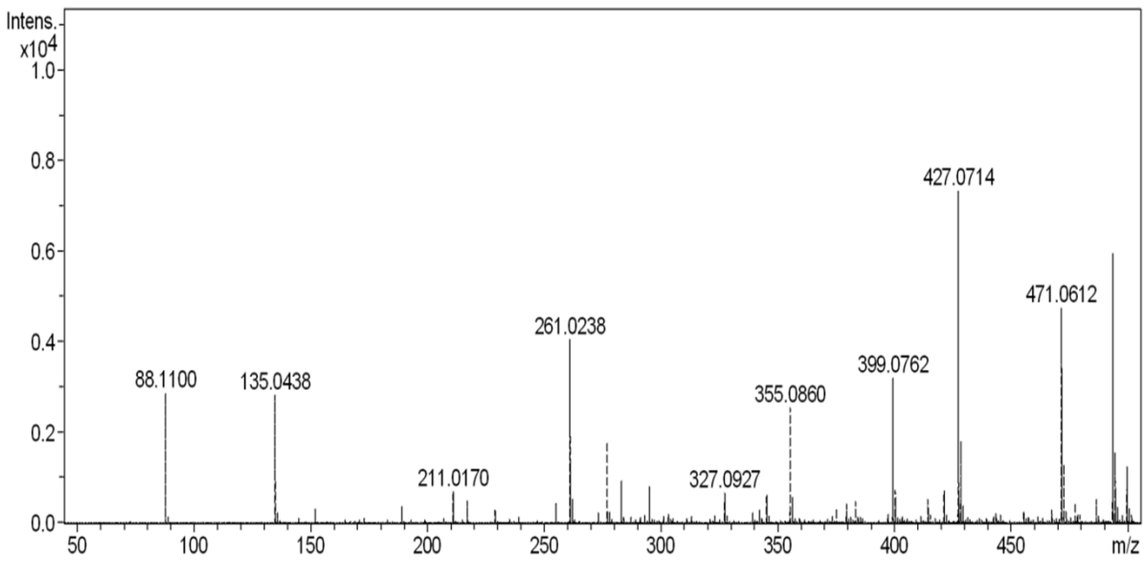

SUPPLEMENTARY 3. ESI-MS spectra of EOQA

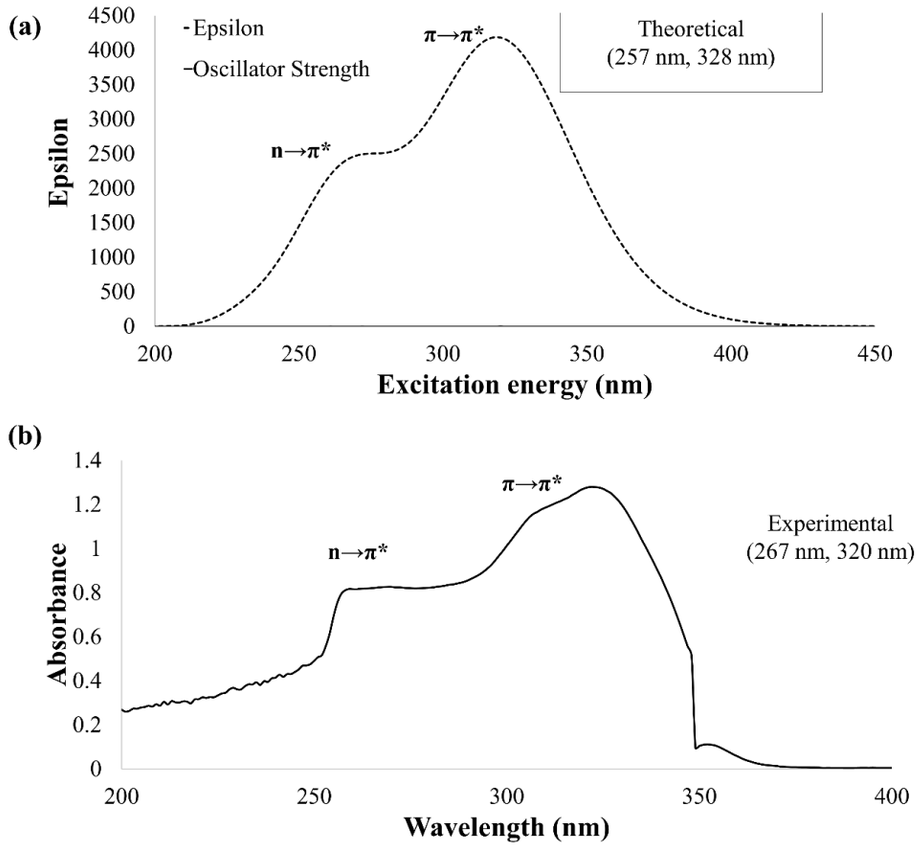

SUPPLEMENTARY 4. UV-Vis spectrum of OQAA between theoretical and experimental (a) Theoretical electronic absorption spectra of OQAA (257 nm, 328 nm), and (b) Experimental absorbance of OQAA (267 nm, 320 nm)

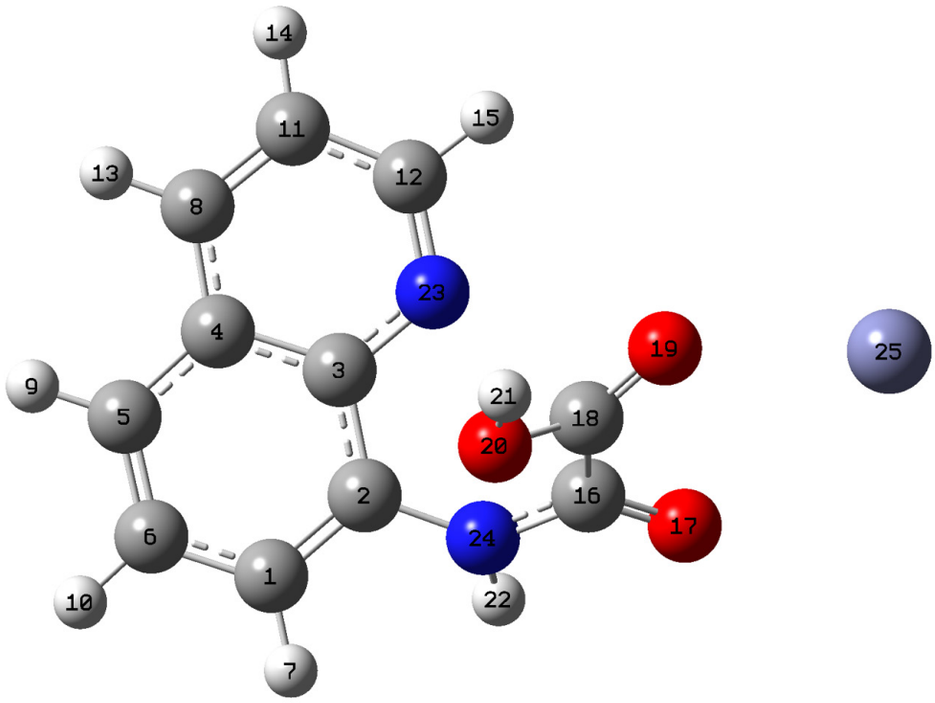

SUPPLEMENTARY 5. The optimized molecular geometry of OQAA-Zn complex at DFT/B3LYP/GEN/LANL2DZ). Dark grey, light grey, red, blue, and shady purple spheres refer to C, H, O, N, and Zn